Use of Dielectric material in Muon Accelerator RF Cavities

by

Katheryn Decker French

Submitted to the Department of Physics
in partial fulfillment of the requirements for the degree of

Bachelor of Science in Physics

at the

MASSACHUSETTS INSTITUTE OF TECHNOLOGY

June 2011

Author .....
Department of Physics
April 26, 2011

Certified by .....
William Barletta
Adjunct Professor, Departments of Physics
Thesis Supervisor

Certified by .....
Milorad Popovic
Fermilab
Thesis Supervisor

Accepted by .....
Professor Nergis Mavalvala
Senior Thesis Coordinator, Department of Physics

Use of Dielectric material in Muon Accelerator RF Cavities

by

Katheryn Decker French

Submitted to the Department of Physics
on April 26, 2011, in partial fulfillment of the
requirements for the degree of
Bachelor of Science in Physics

Abstract

The building of a muon collider is motivated by the desire to collide point-like particles while reducing the limitations imposed by synchrotron radiation. The many challenges unique to muon accelerators are derived from the short lifetime of the muons. The muons must be produced, then formed into a beam and accelerated to their final energy in less than a few milliseconds in the lab frame. One idea for accomplishing this is called a helical cooling channel (HCC), and requires placing the accelerating structure in a solenoid. The RF (radio frequency) accelerating structure in a muon accelerator should be short in the longitudinal direction, small enough in the transverse direction to fit inside the solenoids of the helical cooling channel, and have the highest possible electric field gradient. A RF cavity that meets these requirements is crucial to the development of a muon collider. There is an additional constraint if an existing source of RF power is to be used, as the frequency of the lowest RF cavity mode should match the frequency of the power source. At Fermilab, the klystrons produce RF power at 800MHz. The resonant frequency of an RF cavity depends inversely on the radius of the cavity, as well as the dielectric constant of the material within the cavity. A standard vacuum cavity with a resonant frequency of 800 MHz is too large to fit within the solenoids. This paper studies one method of avoiding this limitation by placing a dielectric material within the cavity. Another problem faced by a cavity within an HCC is the effect of the magnetic field. The solenoid field will serve to focus electrons emitted from the sides of the cavity, causing breakdown at lower electric fields than those possible without the solenoid. By inserting the dielectric at a high electric field point, electrons emitted from the wall behind the dielectric will be attenuated before they can avalanche and cause breakdown.

The effect of this dielectric is modeled in Microwave Studio to determine the right size and shape for the dielectric given, and several prototype cavities are built and tested with a network analyzer. Our proof of concept experiment shows the feasibility of further developing the design of dielectric loaded RF cavities. A design for a cavity to be used at higher power is discussed, along with the testing procedures that will be followed.

Thesis Supervisor: William Barletta
Title: Adjunct Professor, Departments of Physics

Thesis Supervisor: Milorad Popovic
Title: Fermilab

Acknowledgments

I would like to acknowledge Milorad Popovic for advising me throughout this project; Professor Barletta for guiding me in the writing and understanding of the experiment, and providing a great deal of professional advice; and Andrew Feld and Mitch Adamus for helping me build the prototype cavities.

Contents

1 Introduction **15**

1.1 Background 15

1.2 Purpose of Dielectric Material 16

1.3 Overview of Sections 17

2 Muon Collider **19**

2.1 Motivations 19

2.2 Ionization Cooling 20

2.3 Helical Cooling Channel 21

3 Cavity Tuning **23**

3.1 Use of RF in accelerators 23

3.2 Simple Pillbox 24

3.3 Ferrite Tuners 27

3.3.1 Use in low energy proton and heavy ion synchrotrons 28

3.4 Effect of Dielectric on the Quality Factor 28

4 Design in Microwave Studio **31**

4.1 Algorithms used to Calculate Eigenmodes 31

4.2 Effects of Mesh Size on Calculations 31

4.3 Calculation of S- Parameters 32

4.4 Simulation of prototype cavity 34

5 Building Cavity Prototype **39**

6 Testing of Prototype with Network Analyzer **43**

6.1 Measurements 43

6.2 Discussion of Results 44

6.2.1 Frequency Measurements 44

6.2.2 Q Measurements 44

6.3 Discussion 45

7 Design of High Power Cavity **49**

7.1 Vacuum and Power considerations 49

7.1.1 Ports 49

7.1.2 Construction 50

7.2 Importance of High Power Tests 51

7.3 Designs for Future Tests 52

8 Muon Test Area **53**

9 High Power Tests of Cavity **59**

9.1 Conditioning 59

9.2 Quantities Monitored During Tests 60

10 Conclusions **63**

Bibliography **64**

List of Figures

2-1 Schematic of Helical Cooling Channel and RF cavities. (Source: [21]) 21

3-1 Diagrams of the lowest mode of a simple pillbox cavity. The dominant electric field is in the z direction, and the dominant magnetic field is in the theta direction. The left hand picture shows a basic pillbox cavity, while the right hand picture shows a cavity with curved sides (Image Source: [3]). 24

3-2 Plot of the intensity of the E_z and B_θ components of the resonant mode fields with respect to the radial distance from the cavity center (Image Source: [3]). 27

3-3 Image Source: [18]. 28

4-1 Geometry of first cavity in simulation with mesh overlaid. There are about 100,000 mesh cells in this simulation. This is the mesh size used for the simulations with results presented in this paper. 32

4-2 Geometry of first cavity in simulation with different meshes overlaid. There are about 200,000 mesh cells in the top simulation, and 16,000 cells in the bottom. 33

4-3 Geometry of first cavity in simulation. The picture on the right shows a cutout. The yellow is copper, the blue is vacuum, and the pink is ceramic. The background material is perfectly conducting. 35

4-4 Waveguide ports over coaxial antennas in simulation. The ports appear as red squares. 35

4-5 S- parameters for simulation of cavity build 1. S21 is on the top, and S11 is on the bottom. 36
4-6 Results from simulated E field probe in longitudinal direction for simulation of cavity build 1. The y-axis is electric field in V/m. 37

5-1 Photo of existing copper pipe with ceramic insert (left), and photo of cavity, preliminarily held together with copper tape (right). 40
5-2 Photos of antenna (left), and placement of antennas in cavity (right). 40
5-3 Schematic of cavity. 41

6-1 Photo of cavity attached to network analyzer for measurements. . . . 46
6-2 Network analyzer measurement of S21 of the first build of the cavity. The horizontal scale is from 3 kHz to 3 GHz. The vertical scale is in units of 20 dB/division. 47
6-3 Network analyzer measurement of S21 of the first build of the cavity. The horizontal scale is centered at 836.45 MHz with a span of 3 MHz. The vertical scale is in units of 5 dB/division. 47

7-1 Example schematic of RF ports. The central knobs are for materials testing, and would not be included in this experiment. Image Source: Katsuya Yonehara. 50
7-2 Photo of cavity described in Figure 9-1. Image Source: Katsuya Yonehara. 51

8-1 Schematic of MTA Experimental Hall (Image source: [17]) 54
8-2 Ground level view of MTA. 54
8-3 MTA beamline 55
8-4 Front view of solenoid and RF power feed in MTA. For orientation, the beamline comes from the back right in this picture. 55
8-5 Closer view of solenoid, from the side. 56
8-6 Closer view of solenoid and RF feed, again from the side. 56
8-7 Thesis author, in the MTA Experimental Hall. 57

9-1 Example Schematic of High Powered Tests at the MTA(Source: [20]) 61
9-2 Sample observation of a breakdown event. From top to bottom, the signals are: forward RF power, reflected RF power, PMT signal, and electric pickup (Source: [7]). 61

List of Tables

4.1 Results from Microwave Studio simulation of the resonant mode frequencies and quality factors for the three cavities, assuming $\epsilon = 9.7$ and $\tan\delta = 0.0001$. 34

6.1 Results from network analyzer measurements of cavity prototypes. . . 45

6.2 Results from Microwave Studio simulation of the resonant mode frequencies for the three cavities, assuming $\epsilon = 9.7$ and $\tan\delta = 0.0004$, from observations, and the values of ϵ required to reconcile these discrepancies. 45

6.3 Summary of factors affecting the measured frequency of the cavities. 45

6.4 Summary of factors affecting the measured Q factors of the cavities. 46

Chapter 1

Introduction

1.1 Background

Particle accelerators have been responsible for driving much of the recent research in nuclear physics. Colliding particles allows us to probe the structure and properties of matter. Particles and states which are not seen at low energies can be observed for short periods of time at very high energies. Research in accelerator physics generally focuses on methods of increasing the energy of particle collisions and the luminosity (proportional to the rate) of collisions. This project aims to solve one of the challenges of building a muon collider, which could allow very high energy collisions.

Muons are elementary particles similar to electrons, but with a greater mass. Muons are unstable particles, and decay within several milliseconds, so they are not observed in ordinary materials. They can, however, be produced in collisions. A muon collider would need to produce muons, form them into a beam, accelerate them to their final energy, and collide them before they decay. The lifetime of a muon at rest is about 2 microseconds, and is still only on the order of milliseconds in the lab frame when accelerated to TeV range energies.

The idea of a muon collider is motivated by the desire to collide point-like particles at multi-TeV energies while reducing the problem of synchrotron radiation. Accelerating charges lose power through synchrotron radiation proportional to $\frac{E^4}{\rho^2 m^4}$, where E is the particle's energy, m is the particle's mass, and ρ is the bending radius of

the bending magnets. Electrons, with their low mass, will lose much more energy to synchrotron radiation than heavier particles such as protons or muons. For this reason, large circular accelerators are typically proton-proton colliders such as the LHC at CERN, or proton-antiproton colliders such as the Tevatron at Fermilab. One issue with colliding protons, is that the collision products are from the interaction between a single quark from each proton. By colliding point-like particles, their full kinetic energy can be used completely to create new particles.

Many challenges unique to muon accelerators derive from the short lifetime of the muons. The muons must be produced, cooled, then accelerated to their final energy in less than a few milliseconds in the lab frame. The muons are produced by aiming a proton beam at a fixed target to produce pions, then allowing the pions to decay into muons. The muons produced in this way occupy a large phase space, and need to be cooled as they are accelerated. A technique called ionization cooling, where particles pass through a scattering medium, can be used to reduce the momentum of the muons in it's direction of travel, while RF (radio frequency) is used to replenish the muon's energy and accelerate the muons in the longitudinal direction. The accelerating structure is surrounded by solenoids which serve to decrease the momentum of high energy muons more than that of low energy muons, decreasing the momentum spread. This entire structure is known as a helical cooling channel [21].

The RF accelerating structure in a muon accelerator should be short in the longitudinal direction, small enough in the transverse direction to fit inside the solenoids of the helical cooling channel, and have the highest possible electric field gradient. A RF cavity that meets these requirements is crucial to the development of a muon collider.

1.2 Purpose of Dielectric Material

There is an additional constraint on the accelerating structure if an existing source of RF power is to be used, as the frequency of the lowest RF cavity mode should match the frequency of the power source. At Fermilab, the klystrons produce RF

power at 800MHz. The lowest mode frequency in a basic pillbox cavity is given by the equation

$$f = \frac{2.405c}{2\pi R\sqrt{\epsilon\mu}} \tag{1.1}$$

where c is the speed of light, R is the radius of the cavity, and ϵ and μ are the relative dielectric constant and magnetic permeability of the material. Since the cavity must be small in the transverse direction, a dielectric can be put inside the cavity to lower the frequency to the desired 800 MHz. Without the dielectric material, the size of the cavity required to have a mode at 800 MHz would be too large to fit inside the solenoids. The current bore size of the solenoid required is about 44 cm, but this does not include space needed for cooling and controls. The cavity radius corresponding to 800 MHz via the above equation is 14 cm, with no added dielectric or magnetic materials.

In a cavity inside a strong solenoid field, electrons emitted from the side of the cavity will be focused to the other side, where they will cascade, causing electric breakdown. It is often undesirable to have dielectric material in accelerating RF cavities, as the material will be heated from the rapid polarization. However, dielectrics can be used to prevent this type of breakdown. The electric field will be the strongest near the dielectric material, so it is the most likely place for breakdown to occur. However, the electrons released from the side of the cavity will be attenuated as they travel through the material, preventing breakdown.

1.3 Overview of Sections

The scope of this thesis is to describe a series of testing and design used in developing a dielectric- loaded RF cavity. A prototype cavity was built, and tested using a network analyzer. The results from this testing were then used to design a cavity capable of operating at high power.

A more detailed background of muon acceleration and radio frequency cavity design are presented in Chapters 2 and 3. The simulation program used to predict the behavior of the devices is described in Chapter 4. The design, building and

testing of the low power prototype is described in Chapters 5 and 6. The adaptation of this design for use in high power tests is described in Chapter 7. The facility used to conduct the high power tests, the Muon Test Area at Fermilab, is described in Chapter 8. The tests planned for the MTA are presented in Chapter 9.

Chapter 2

Muon Collider

2.1 Motivations

As discussed briefly in Chapter 1, two of the main motivations for building a muon collider are to avoid the synchrotron radiation limitation found in electron- positron colliders, and to use the full kinetic energy of the accelerated particles to create new particles. Different interactions can also lead to more precise measurements of certain produced particles [2]. These last two ideas will be developed further in this chapter.

When studying complex particle interactions, it can be simpler and more efficient to observe lepton collisions. These collisions are single-particle interactions, unlike hadron collisions. When hadrons collide, the quarks rather than the protons or antiprotons (or other hadron) are what interact with each other. This means that the entirety of the kinetic energy of the particles, which is twice the energy imparted during acceleration, is not available for particle creation, as only the kinetic energy of the interacting quarks is available. In addition, interactions between gluons results in a background of particle interactions which obscures other interactions one may wish to observe [8].

One of the most sought-after observations in physics today is the Higgs boson. There are several particle decay channels that are theoretically capable of producing a Higgs. One of these, the s-channel [2], is more readily observable with a muon collider, because the coupling of the interaction is proportional to the mass. This

means that the cross section will scale as the square of the mass, so a muon collider will have an advantage of a factor of about $(207)^2$ over an electron collider [8].

2.2 Ionization Cooling

Muons are produced by colliding protons into a target to produce pions, then allowing the pions to decay into muons, via the weak decay $\pi^- \rightarrow \mu^- + \bar{\nu}$. The muons produced by this method have a very large emittance (proportional to phase space area) in all directions, and must be cooled into a beam. Because of the short lifetime of the muons, this cooling process must take place within milliseconds. One method of cooling favored for muon accelerators is ionization cooling [10] [9] [14]. During ionization cooling, the muons pass through a material, where their momentum is lowered in all 3 directions, then an accelerating cavity, where the longitudinal momentum is increased. This sequence is repeated several times. The transverse emittance must be reduced by a factor of about 300 in both x and y, and longitudinal emittance must be reduced by a factor of 10. The total reduction in phase space must be on the order of a factor of 10^6 [8]. Transverse emittance refers to the variations in x and y positions and momenta, for a beam traveling in the z direction. A beam with lower emittance will be able to maintain a small area as it travels through the Longitudinal emittance refers to the tightness of the "bunches" in the beam cause by the phase of the RF acceleration. Because the RF system can only accelerate particles during half of its cycle, the particles will be bunched in phase with the RF. Longitudinal emittance is also affected by variations in the energy of the particles, as faster particles will advance their phase from cycle to cycle. A system reducing the longitudinal emittance should be constructed such that higher momentum muons are cooled more than lower momentum muons in the longitudinal direction.

Other methods of cooling particle beams are unsuitable for cooling muons. Radiation damping, using the synchrotron radiation given off to expel energy, is unavailable due to the large mass of the muon. Stochastic cooling, in which the beam properties on one side of the ring are measured, then corrected for on the other side, is too slow

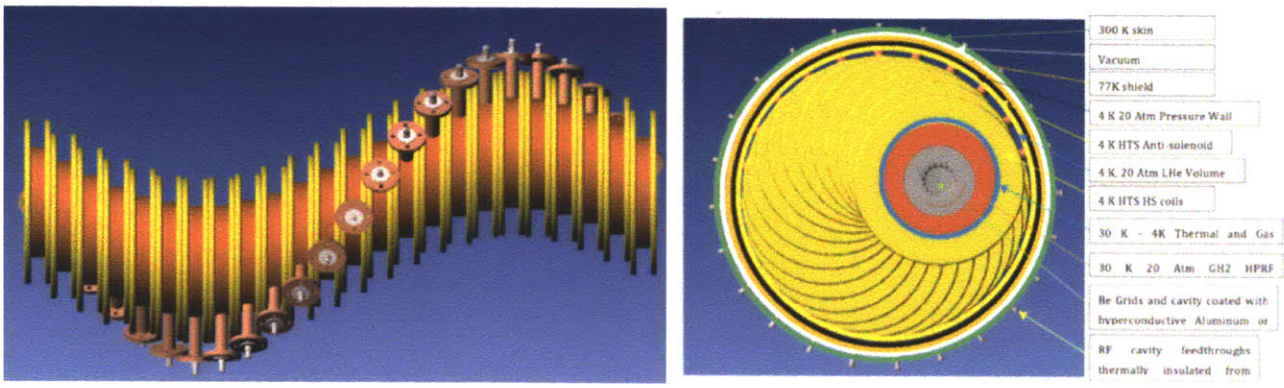

Figure 2-1: Schematic of Helical Cooling Channel and RF cavities. (Source: [21])

for this application [8].

Some considerations for ionization cooling are reducing the heating due to scattering in the material, and aiding in the longitudinal emittance reduction. The cooling from muons ionizing the material must be greater than the heating from multiple scattering in the material in order for the cooling effect to dominate. This can be accomplished by using low- Z materials and a strong focusing field.

2.3 Helical Cooling Channel

The Helical Cooling Channel (HCC) is a method of reducing the longitudinal emittance of the muon beam [21] [6]. A diagram is shown in Figure 2-1. The HCC uses solenoid, helical dipole, and helical quadrupole components to provide a magnetic field which will give continuous non-zero dispersion [1] for the muon beam. Higher energy muons will travel a longer path length than lower energy muons, causing the higher energy muons to lose a greater amount of energy. This will result in a further reduction in the transverse emittance. A detailed analysis of the HCC can be found in [6].

[1]Dispersion describes the effect of a spread in momentum, and is written $D = \frac{p}{a}\frac{da}{dp}$ where p is the momentum, and a is the radius of the helix [6].

Chapter 3

Cavity Tuning

3.1 Use of RF in accelerators

There are two approaches to accelerating charged particles, DC and AC. Particles will accelerate when placed in an electric field. This field can be generated between a high voltage source and ground. The strength of the field which can be created is limited by the practicality of building high voltage sources. The problem can be overcome through clever means such as with a Cockcroft-Walton machine [4] but it is still very difficult to maintain high voltages. DC acceleration is often used to begin the process of acceleration, but is seldom used in the main accelerator. Generating high oscillating electric fields is much easier than generating a high static electric field. One can set up a cavity with an oscillating electric field such that a particle will pass through the electric field in the accelerating phase, and be shielded from the field when in the decelerating phase. Radio frequency (RF) cavities are one way of implementing this AC method.

An RF cavity converts an alternating current source (with a frequency in the radio to microwave range) to an oscillating electric field in the desired direction. Each cavity will have a set of resonant modes, for which the input power will result in the largest response in the magnitude of the electric and magnetic fields. An example of the lowest mode of a cavity can be seen in Figure 3-1. Because of this, it is important to match the frequency of the power source with that of the cavity. The resonant mode

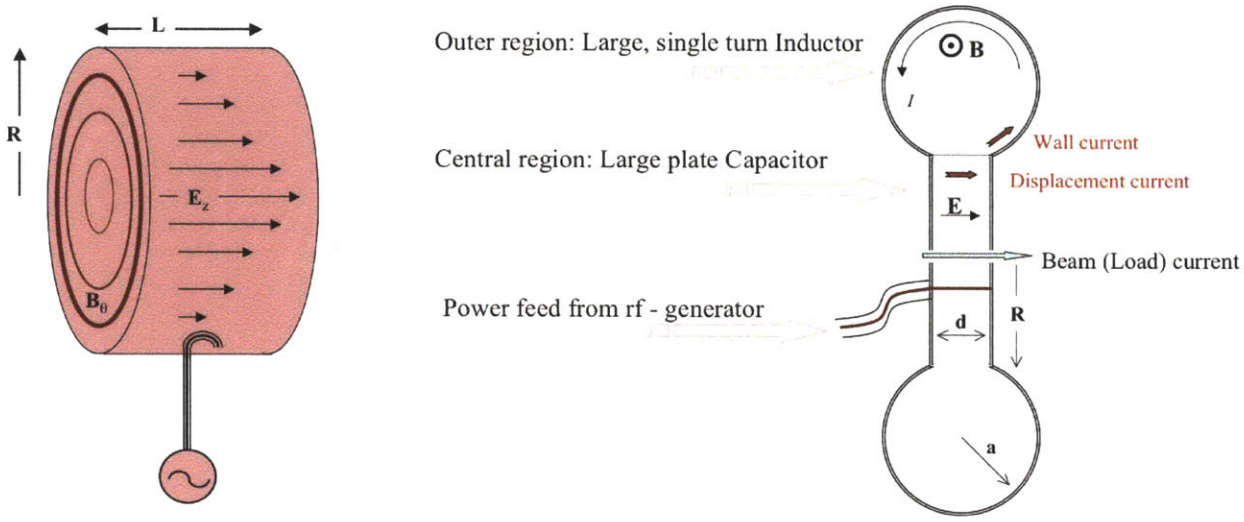

Figure 3-1: Diagrams of the lowest mode of a simple pillbox cavity. The dominant electric field is in the z direction, and the dominant magnetic field is in the theta direction. The left hand picture shows a basic pillbox cavity, while the right hand picture shows a cavity with curved sides (Image Source: [3]).

frequencies of the cavity depend on the geometry and materials used, which will be shown in the following section.

3.2 Simple Pillbox

RF cavities are essentially circular waveguides using TM (transverse magnetic field) modes. These modes can be derived using Maxwell's equations and the boundary conditions of the cavity. For a basic pillbox cavity (see Figure 3-1), this can be done analytically. For a TM mode, the electric field will be in the longitudinal direction (z), and the magnetic field will curl around this in the transverse plane. Their solutions will be in the form of bessel functions, and the lowest resonant frequency can be determined by finding the first zero of the bessel function appropriate for the boundary conditions. What follows is a brief derivation of the resonant mode frequency of a basic pillbox cavity. [11] [13]

TM010 is the lowest TM mode, and will have a magnetic field in the transverse directions, with $Hz = 0$, and an electric field in the z- direction only.

CGS units will be used throughout. Assuming the absence of free charges and a

$exp(j\omega t)$ time dependence of the fields, Maxwell's equations are:

$$\nabla \bullet B = 0, \nabla \times E = j\frac{\omega}{c}B, \nabla \bullet E = 0, \nabla \times B = -j\mu\varepsilon\frac{\omega}{c}E. \tag{3.1}$$

The two curl equations can be broken up into their components to get six equations. Assuming a propagation in the z- direction of $\exp -i\beta z$, one can solve for the transverse field components in terms of the longitudinal field components. It will be convenient to use cylindrical coordinates due to the cylindrical symmetry of the problem.

$$E_\rho = -\frac{j}{{k_c}^2}\left(\beta\frac{\partial E_z}{\partial\rho} + \frac{\omega\mu}{\rho c}\frac{\partial H_z}{\partial\phi}\right), \tag{3.2}$$

$$E_\phi = \frac{-j}{{k_c}^2}\left(\frac{\beta}{\rho}\frac{\partial E_z}{\partial\phi} - \frac{\omega\mu}{c}\frac{\partial H_z}{\partial\rho}\right), \tag{3.3}$$

$$H_\rho = \frac{j}{{k_c}^2}\left(\frac{\omega\epsilon}{\rho}\frac{\partial E_z}{\partial\phi} - \frac{\beta}{c}\frac{\partial H_z}{\partial\rho}\right), \tag{3.4}$$

$$H_\phi = -\frac{j}{{k_c}^2}\left(\omega\epsilon\frac{\partial E_z}{\partial\rho} + \frac{\beta}{\rho c}\frac{\partial H_z}{\partial\phi}\right) \tag{3.5}$$

where ${k_c}^2 = k^2 - \beta^2$, and $k = \omega\sqrt{\mu\epsilon}$.

Equation 3.1 can also be used to derive equations for electromagnetic wave propagation:

$$\left(\nabla^2 + \mu\varepsilon\frac{\omega^2}{c^2}\right)E = 0, \left(\nabla^2 + \mu\varepsilon\frac{\omega^2}{c^2}\right)B = 0 \tag{3.6}$$

which can again be separated into equations for each orthogonal component.

Because we are considering the TM modes, we will use the equation for electric field propagation. This gives an equation for E_z,

$$\left(\frac{\partial^2}{\partial\rho^2} + \frac{1}{\rho}\frac{\partial}{\partial\rho} + \frac{1}{\rho^2}\frac{\partial^2}{\partial\phi^2} + \frac{\partial^2}{\partial z^2} + \mu\varepsilon\frac{\omega^2}{c^2}\right)\mathrm{E_z} = 0. \tag{3.7}$$

We will assume that the field solutions are separable, and can be written as

$$\mathrm{E_z} = R(\rho)Q(\phi)e^{-j\beta z + j\omega t} \tag{3.8}$$

and that the variation in ϕ can be expressed by plane waves

$$Q(\phi) = e^{\pm im\phi}. \tag{3.9}$$

The differential equation now becomes

$$\left(\frac{\partial^2}{\partial\rho^2} + \frac{1}{\rho}\frac{\partial}{\partial\rho} - \frac{m^2}{\rho^2} - \beta^2 + \mu\varepsilon\frac{\omega^2}{c^2}\right) R(\rho) = 0. \tag{3.10}$$

Solutions to this differential equation are bessel functions.

$$R(\rho) = AJ_m(\gamma\rho) + BY_m(\gamma\rho), \tag{3.11}$$

$$\gamma^2 = \mu\varepsilon\frac{\omega^2}{c^2} - \beta^2 \tag{3.12}$$

We now have an equation for E_z,

$$\mathrm{E_z}(\rho, \phi, z, t) = \left(AJ_m(\gamma\rho) + BY_m(\gamma\rho)\right) e^{-j\beta z + j\omega t}. \tag{3.13}$$

Because we are concerned with the lowest mode of the cavity, $m = 0$.

For a cavity made of some dielectric, surrounded by a perfectly conducting material, the Y bessel functions will be unphysical, since they go to infinity at 0, $Y_m(0) = \infty$. Thus the electric field will be

$$\mathrm{E}_\rho = 0, \mathrm{E}_\phi = 0, \mathrm{E_z} = E_0 J_0(\gamma\rho) e^{-j\beta z + j\omega t}. \tag{3.14}$$

The electric and magnetic fields will look like those in Figure 3-2, when their intensity is plotted against the radius of the cavity.

To find the value of ω, we find the location of the first zero in the bessel function. This is just a constant, which depends on m. For m=1, the first zero $J_0(x) = 0$ is at x=2.405. Because n=1, this first zero will occur at the boundary. For a cylinder of radius a,

$$J_0(\gamma a) = 0 \tag{3.15}$$

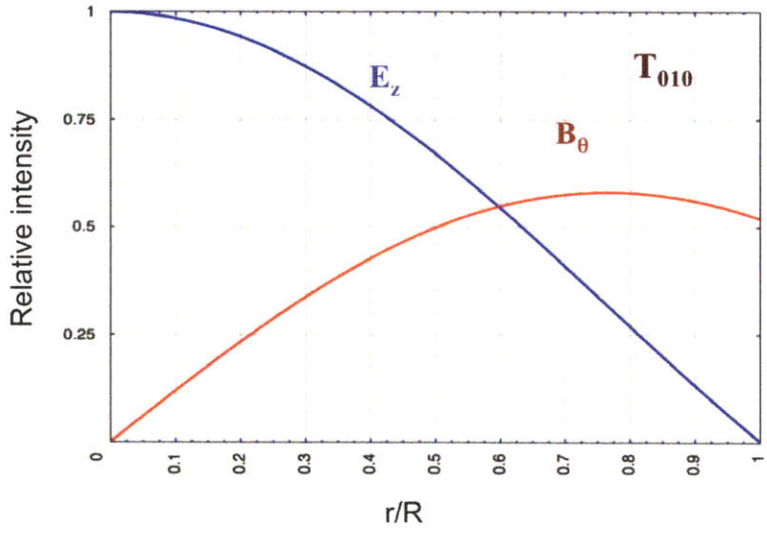

Figure 3-2: Plot of the intensity of the E_z and B_θ components of the resonant mode fields with respect to the radial distance from the cavity center (Image Source: [3]).

$$\gamma a = 2.405. \tag{3.16}$$

Remembering that $\gamma^2 = \mu\varepsilon\frac{\omega^2}{c^2} - \beta^2$and solving for the frequency $f = \frac{\omega}{2\pi}$,

$$f = c\frac{\sqrt{\frac{2.405^2}{a^2} + \beta^2}}{2\pi\sqrt{\varepsilon\mu}} \tag{3.17}$$

For the TM010 mode, $\beta = 0$, so

$$f = \frac{2.405c}{2\pi a\sqrt{\epsilon\mu}} \tag{3.18}$$

3.3 Ferrite Tuners

One of the motivations for changing the ϵ of the cavity, is the precedent of using temperature-dependent μ (magnetic permeability) materials in cavities. Using these materials, the cavity can be easily tuned. This is useful for increasing the frequency of a cavity as a beam gains energy, as must be done in a synchrotron.

Unfortunately, this method cannot be used for the application of this thesis, as the cavity must be placed inside a solenoid, where it will be subject to a strong magnetic

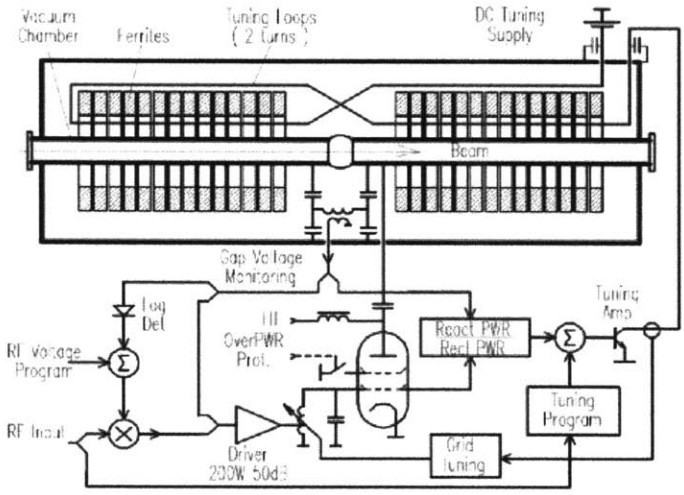

Fig. 3: Principal diagram of the tuneable ferrite cavity assembly and control [16].

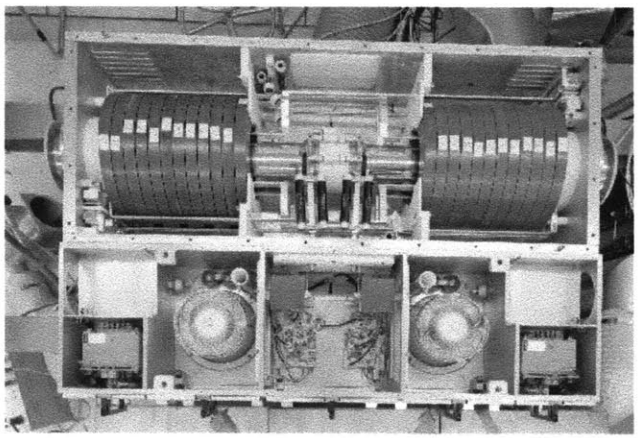

Fig. 2: Ferrite loaded accelerating cavity used in the PSB (picture taken in 1983). The beam passes in the horizontal direction inside the vacuum chamber surrounded by massive ferrite rings. The two tetrodes are located at the bottom of the metallic chassis that includes the ensemble.

Figure 3-3: Image Source: [18].

field.

3.3.1 Use in low energy proton and heavy ion synchrotrons

Cavities with easily adjustable frequency are useful in synchrotrons and low energy proton accelerators, where the velocity of the particles is much less than the speed of light. Tuning the cavity allows for the particle bunches to remain in phase with the RF power as they are accelerated. A good example of the use of ferrite tuned cavities can be seen in CERN's Proton Synchrotron Booster (PSB) and Proton Synchrotron (PS) [18]. A diagram and picture of a ferrite tuner from the PSB can be seen in Figure 3-3.

3.4 Effect of Dielectric on the Quality Factor

One measure of a system's ability to store energy is Q, the quality factor. It is defined as

$$Q = \frac{\omega W}{P_{loss}} \tag{3.19}$$

where ω is the frequency, W is the energy lost per cycle, and P_{loss} is the power lost. For a dielectric loaded cavity, Q is a measure of the heat loss of the design. Much of the power will be lost in the dielectric. The above equation can be broken up into power lost into the dielectric and the wall of the cavity using $P_{loss} = P_{wall} + P_{diel}$ [12].

This results in the equation for Q:

$$\frac{1}{Q} = \frac{1}{Q_{wall}} + \frac{1}{Q_{diel}}. \tag{3.20}$$

The Q of the dielectric is given by the loss tangent, as $Q_{diel} = 1/tan\delta$. For example, the loss tangent of Alumina used in later simulations is 0.0001, which corresponds to a Q of 10,000 if no geometric factors are accounted for. The Q of the dielectric is expected to be the dominant factor in the Q of a dielectric loaded cavity, so this can be used to determine the maximum loss tangent a dielectric material can have in order to be feasible for an RF cavity in a muon accelerator.

Chapter 4

Design in Microwave Studio

A program called Microwave Studio, made by CST is used to simulate the electric and magnetic fields inside the cavity. The geometry of the cavity can be drawn, with materials of specified properties. Two analyses are done of the cavity. The first uses the eigenmode solver to calculate the resonant frequency of the cavity and the quality factor. The second uses the transient solver to calculate the S- parameters, which describe the power transported through the device, by modeling the power inputs through the cavity's antennas.

4.1 Algorithms used to Calculate Eigenmodes

Microwave studio uses two main algorithms to calculate eigenmodes of a system: Advanced Krylow Subspace (AKS), and Jacoby Davidson Method (JDM). The AKS method is faster, and thus will be able to calculate more of the higher modes of a system in a more reasonable time, while the JDM method is potentially able to include materials losses into the calculation [5].

4.2 Effects of Mesh Size on Calculations

The calculation programs divide the model with a mesh in order to calculate S parameters and Eigenmodes. In the simulations for this experiment, the mesh was refined

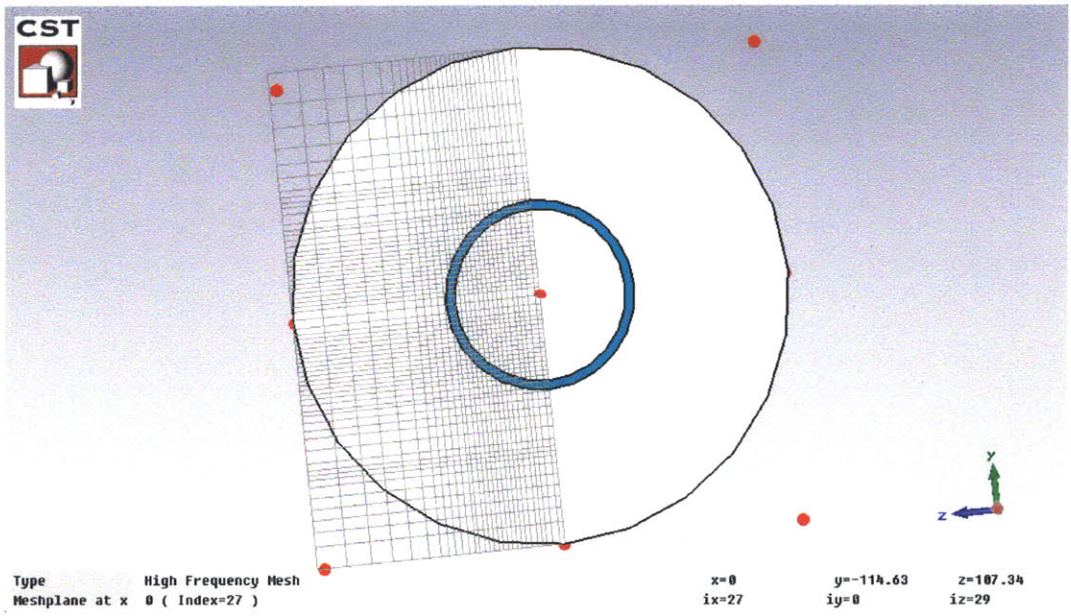

Figure 4-1: Geometry of first cavity in simulation with mesh overlaid. There are about 100,000 mesh cells in this simulation. This is the mesh size used for the simulations with results presented in this paper.

around the material boundaries and dielectric. A picture of the mesh superimposed on the cavity can be seen in Figure 4-1. Simulations were run with various mesh sizes, in order to determine the effect of the mesh size. The mesh shown in Figure 4-1 has 10 lines per wavelength, which corresponds to 100,000 cells. A higher density mesh (13 lines/wavelength, 200,000 cells), shown in Figure 4-2 produced the same mode frequency, with a lower Q, and a lower density mesh (7 lines/wavelength, 16,000 cells) produced a lower mode frequency, and an intermediate Q. Meshes with 6 or less lines per wavelength were too small to meet the accuracy demands of the solver.

4.3 Calculation of S- Parameters

S-parameters describe the relation between the input and output voltages of a system. For a system with two ports, the input and output voltages are related by the matrix equation:

$$\begin{pmatrix} b1 \\ b2 \end{pmatrix} = \begin{pmatrix} S11 & S12 \\ S21 & S22 \end{pmatrix} \begin{pmatrix} a1 \\ a2 \end{pmatrix} \tag{4.1}$$

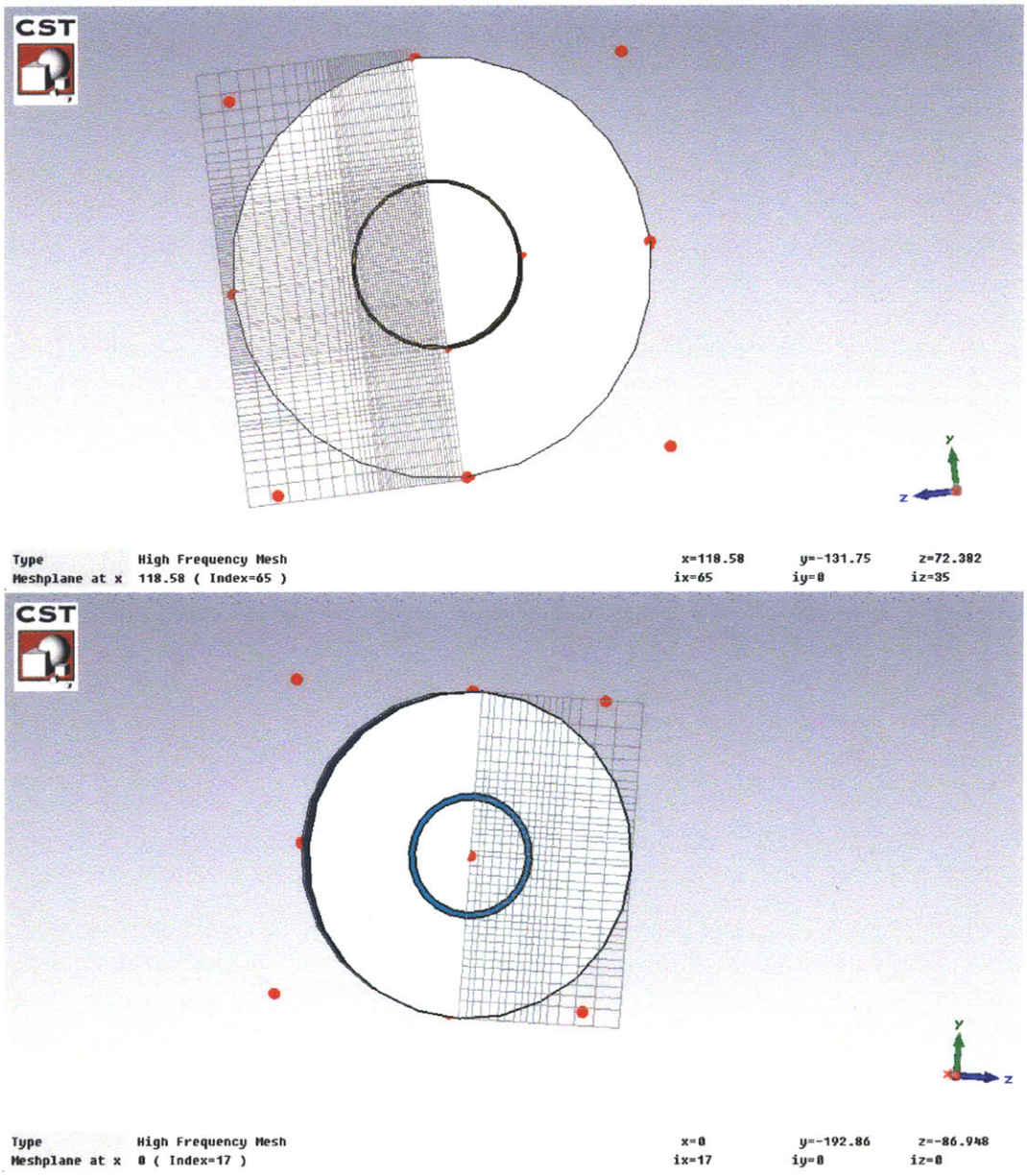

Figure 4-2: Geometry of first cavity in simulation with different meshes overlaid. There are about 200,000 mesh cells in the top simulation, and 16,000 cells in the bottom.

Simulations for three cavity designs

Build	Width (mm)	f_{sim} (MHz)	Q_{wall}	Q_{total}
1	79	789	19,170	6572
2	91	740	19,303	6587
3	86	756	17,793	6402

Table 4.1: Results from Microwave Studio simulation of the resonant mode frequencies and quality factors for the three cavities, assuming $\epsilon = 9.7$ and $\tan\delta = 0.0001$.

where b1 and b2 are output voltages for ports 1 and 2, and a1 and a2 are input voltages. S11 and S22 represent the reflection coefficients for the ports, while S21 represents the forward voltage transmission, and S12 the backwards voltage transmission.

This can be generalized for an N port system, and one can write an NxN matrix. For a reciprocal system, the matrix will be symmetric, and for a lossless system, the matrix will be unitary. By measuring the change in the S-parameter matrix with frequency, the frequency response of the system can be easily understood.

4.4 Simulation of prototype cavity

The geometry of the first build of the cavity input into the model can be seen in Figure 4-3. The radius is 104 mm and the width is 79 mm. The dielectric has a relative dielectric constant of 9.7. The simulation predicts a resonant frequency of 789 MHz. The eigenmode solver uses the AKS (Advanced Krylow Subspace) algorithm, and ignores the losses in the materials when calculating the frequency. A separate solver is used to find the Q. For this simulation, the loss tangent of the material is $\tan(\delta) = 0.0001$. The Q is calculated to be $Q = 6572$ for the lowest mode. The simulated data for other builds of the cavity can be seen in Table 4.4.

The power input into the cavity is simulated using waveguide ports over coaxial antennas, and is shown in Figure 4-4. The transient solver calculates the fields and energy transmission in the time domain. The predicted S-parameters as a function of frequency over the range of 0.1 to 2 MHz can be seen in Figure 4-5. An electric field probe is placed in the center of the cavity to record the magnitude of the electric field

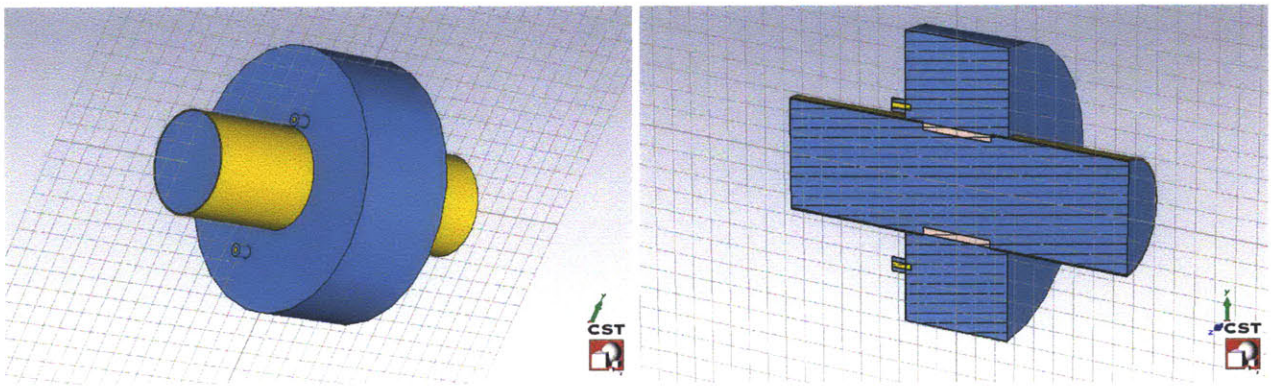

Figure 4-3: Geometry of first cavity in simulation. The picture on the right shows a cutout. The yellow is copper, the blue is vacuum, and the pink is ceramic. The background material is perfectly conducting.

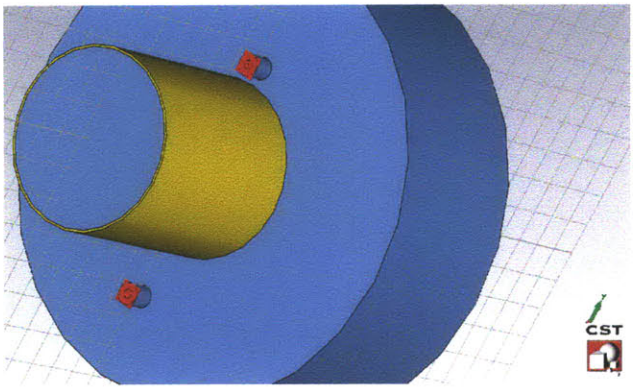

Figure 4-4: Waveguide ports over coaxial antennas in simulation. The ports appear as red squares.

in the longitudinal direction. The results from this probe can be seen in Figure 4-6.

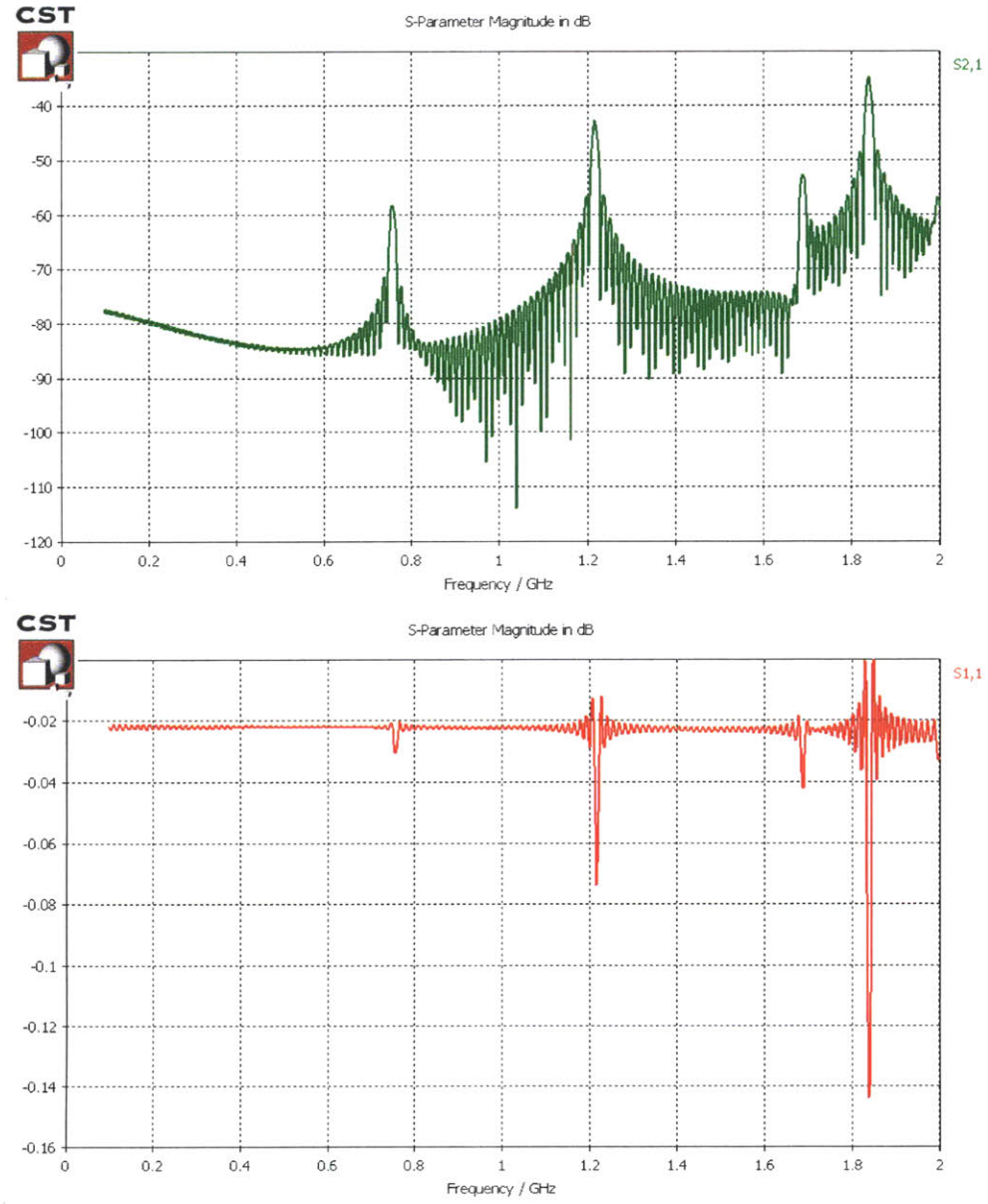

Figure 4-5: S- parameters for simulation of cavity build 1. S21 is on the top, and S11 is on the bottom.

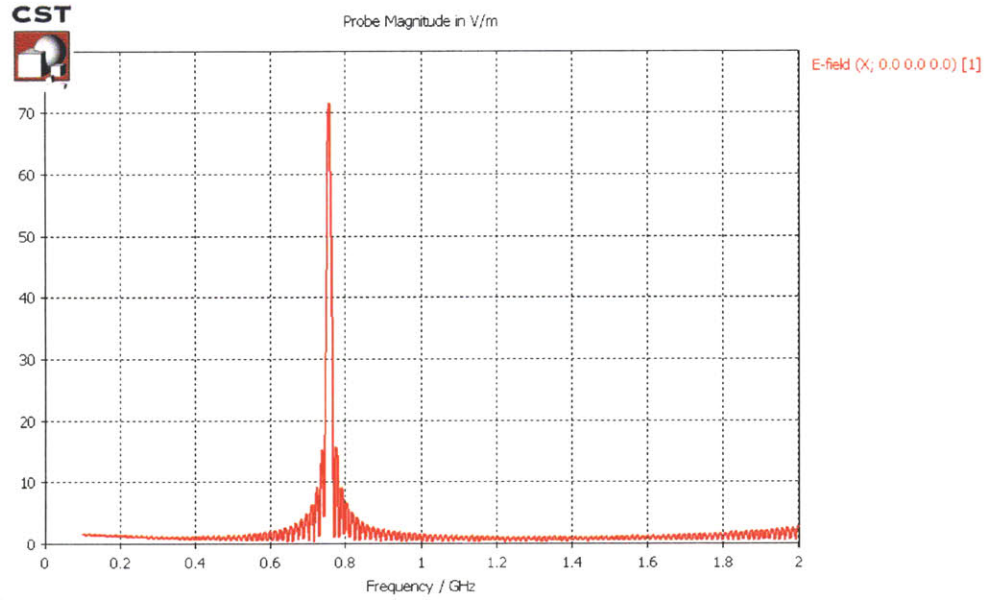

Figure 4-6: Results from simulated E field probe in longitudinal direction for simulation of cavity build 1. The y-axis is electric field in V/m.

Chapter 5

Building Cavity Prototype

The cavity was constructed around an existing setup of a ceramic cylinder between two copper pipes, shown in Figure 5-1. The ceramic was attached using a vinyl acetate seal. Alumina 99.5% was used for the ceramic. It has a relative dielectric constant of $\epsilon = 9.7$ and a loss tangent of $\tan\delta = 0.0001$ from the manufacturer, measured at 1 MHz [1]. The cavity's outer shell was designed in Microwave Studio, and constructed out of two copper side plates and a strip of copper around the outer edge, resting over the two side plates, as shown in Figure 5-1. Here, the copper side plates are placed slightly wider than the ceramic tube. Power was fed into the cavity and measured using two antennas. The antennas and their placement are shown in Figure 5-2. A labelled schematic of the cavity can be seen in Figure 5-3.

Several different cavity geometries were tested by replacing the center copper strip. Three different widths of this strip were tested in order to compare the measurements of the cavity's resonant mode to simulations. The width, rather than the radius was changed in order to reuse the most components between builds. These subsequent builds of the cavity were again constructed with copper tape. The last attempt was welded together in an attempt to raise the Q of the cavity, but was unsuccessful. The Q of the cavity was consistently measured to be lower than expected (see Chapter 4 for predictions, and Chapter 6 for measurements), but some of this can be attributed to gaps between the side plates and outer copper cylinder. These gaps were present both in the copper tape and (to a lesser extent in the) welded version, and result in a

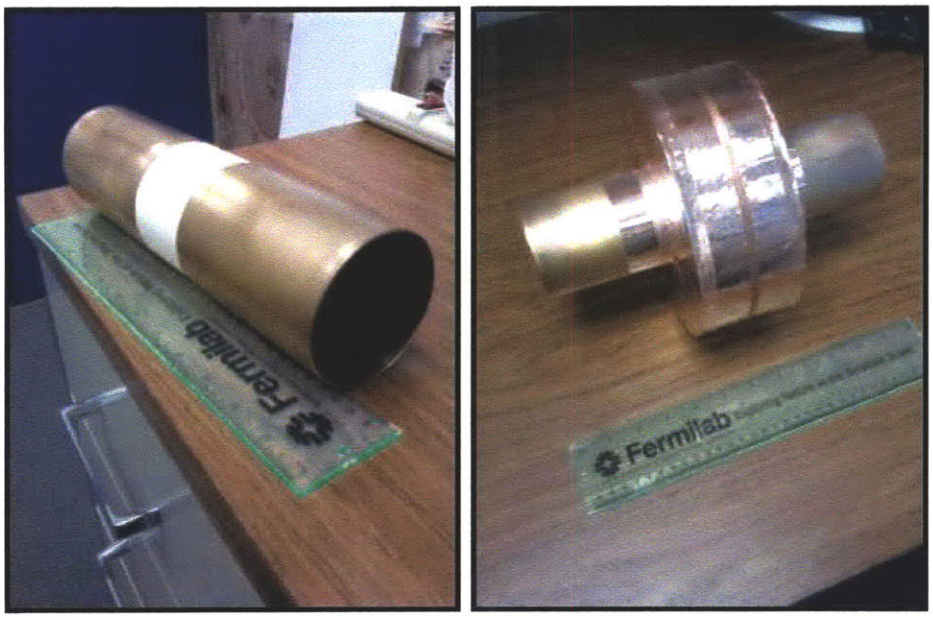

Figure 5-1: Photo of existing copper pipe with ceramic insert (left), and photo of cavity, preliminarily held together with copper tape (right).

Q that reflects the construction of the cavity rather than the presence of the dielectric. Comparisons between the simulated and measured quantities are discussed in Chapter 6, with further analysis.

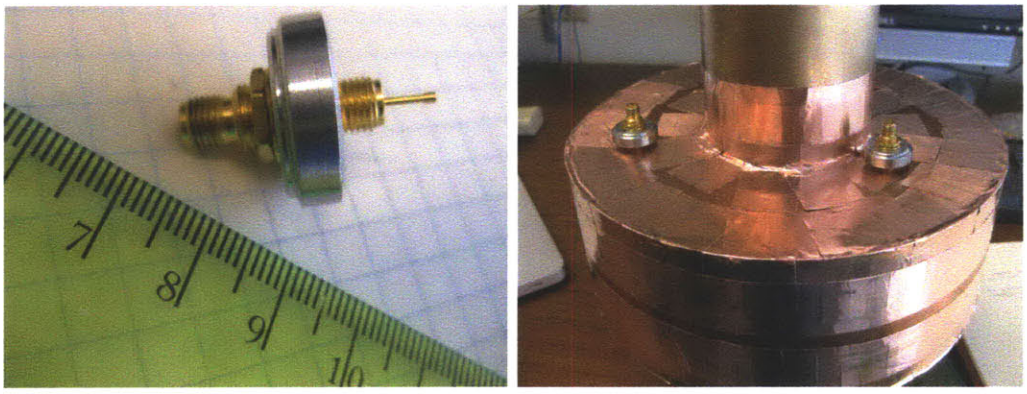

Figure 5-2: Photos of antenna (left), and placement of antennas in cavity (right).

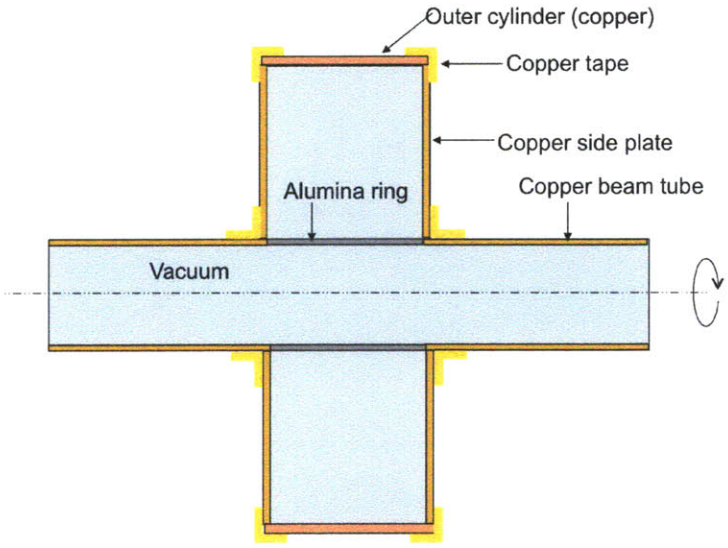

Schematic representation of components of dielectric loaded pill box cavity

Figure 5-3: Schematic of cavity.

Chapter 6

Testing of Prototype with Network Analyzer

6.1 Measurements

Properties of the cavity were measured using a network analyzer. The setup is shown in Figure 6-1. A full two-port calibration was used, as well as time averaging in order to reduce systematic and statistical error respectively.

The resonant frequency and Q were measured for each build of the cavity using the forward transmission parameter S_{21}. The scan over 3 kHz to 3 GHz for the first build can be seen in Figure 6-2, and the close up scan can be seen in Figure 6-3. The width is calculated by finding the points -3 dB from the maximum. The center is calculated to be f = 836.14 MHz, with a bandwidth of bw = 1.43 MHz, and a Q of Q = 583.72. A summary of the results of the network analyzer measurements can be seen in Table 6.1.

6.2 Discussion of Results

6.2.1 Frequency Measurements

The discrepancy between the observed (f = 836 MHz) and simulated (f = 789 MHz) results of the first build prompted the building of subsequent cavities. The cavity was rebuilt twice with different widths between the side plates. The results from network analyzer measurements of these cavities can be seen in Table 6.1. A frequency discrepancy was observed in these cavities similar to the first.

One possible source of the frequency difference could be a change in the dielectric constant at high frequencies. Our measurements provided three data points for determining what ϵ would need to be in order to account for these discrepancies. Results can be seen in Table 6.2. The necessary value is $\epsilon = 7.4 \pm 0.1$. However, this is unlikely, as measurements of alumina's dielectric constant remain constant across a much wider variation in frequencies, through the THz range [19].

Other possibilities for the source of the observed discrepancy are summarized in Table 6.3. The next largest possible source of error after a difference in ϵ is the uncertainty in cavity size. This is due to imperfections in the circular shaping of the cavity. No other effects studied are of a magnitude able to explain the large frequency discrepancy.

6.2.2 Q Measurements

The Q values for each cavity build are seen in Table 6.1. After measuring the third build of the cavity, held together by copper tape, the cavity was soldered shut in order to determine a more realistic value of Q. The Q measured for this cavity was Q = 439. While this is greater than what was observed for the taped cavity with the same dimensions, it is still much lower than the predicted 6000 (see Chapter 4). A summary of the factors affecting Q can be seen in Table 6.4. Unfortunately, filling the gaps in the sides of the cavity with solder decreased the Q, due to the different conductivities of the solder and copper. The decrease of predicted Q with mesh size

Summary of Measurements

Build	Width (mm)	f_{obs} (MHz)	Q
1	79	836	584
2	91	785	178
3	86	807	162

Table 6.1: Results from network analyzer measurements of cavity prototypes.

Simulations and Measurements for three cavity designs

Build	Width (mm)	f_{sim} (MHz)	f_{obs} (MHz)	ϵ
1	79	789	836	7.4
2	91	740	785	7.5
3	86	756	807	7.3

Table 6.2: Results from Microwave Studio simulation of the resonant mode frequencies for the three cavities, assuming $\epsilon = 9.7$ and $\tan\delta = 0.0004$, from observations, and the values of ϵ required to reconcile these discrepancies.

also indicates that the values given in Chapter 4 are overestimates. More precise machining will be required to raise the Q to a value such that it is limited only by the dielectric.

6.3 Discussion

These cold tests are the first step in developing a dielectric loaded cavity for a muon accelerator. The information from these tests is sufficient to guide the next step in development, which will be described in the following three sections. There are several tests and design iterations to be done. The first is to test the cavity at high power. This will enable a more accurate measurement of the frequency and Q, and push the

Summary of errors I (frequency)

Source	Effect on Frequency (MHz)
Uncertainty in dimension measurements of cavity	±27 MHz
Change in dielectric constant by -1	+25 MHz
Size of antennas	+5 MHz
Uncertainty in dimension measurements of ceramic	±3 MHz
Curvature of edges	+1 MHz
Gaps in construction	+1 MHz

Table 6.3: Summary of factors affecting the measured frequency of the cavities.

Summary of errors II (Q)

Source	Effect on Q
Filling gaps with solder	-1400
Effect of doubling mesh cells	-150
Gaps in construction	-30
Uncertainty in dimension measurements of ceramic	±25

Table 6.4: Summary of factors affecting the measured Q factors of the cavities.

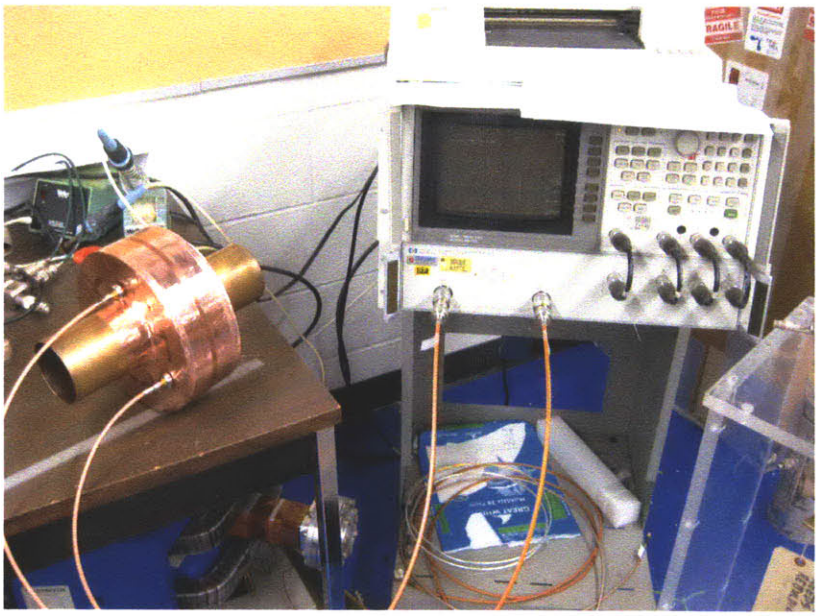

Figure 6-1: Photo of cavity attached to network analyzer for measurements.

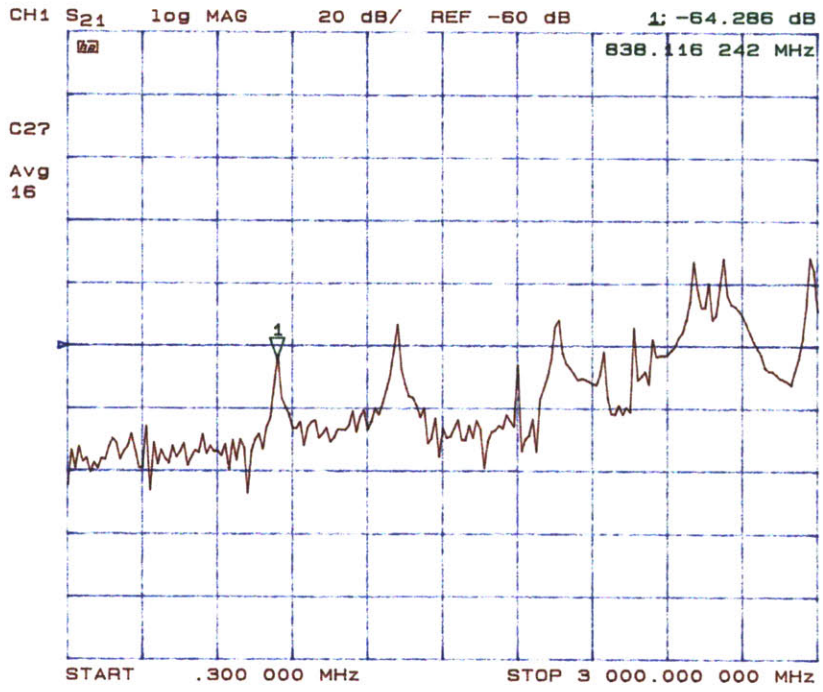

Figure 6-2: Network analyzer measurement of S21 of the first build of the cavity. The horizontal scale is from 3 kHz to 3 GHz. The vertical scale is in units of 20 dB/division.

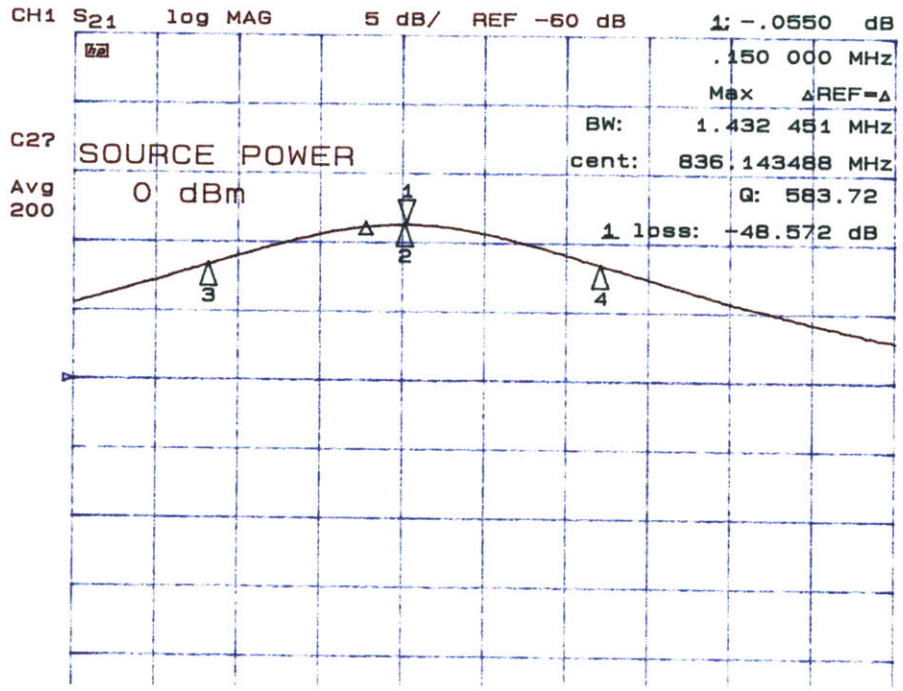

Figure 6-3: Network analyzer measurement of S21 of the first build of the cavity. The horizontal scale is centered at 836.45 MHz with a span of 3 MHz. The vertical scale is in units of 5 dB/division.

design forward. Later tests will be done with a magnetic field. The hope behind the dielectric cavity is that it will lessen the effect of breakdown, which has suppressed the field gradient of other cavities operating in a magnetic field. Eventually, the effect of beam loading on the cavity must be tested.

Chapter 7

Design of High Power Cavity

7.1 Vacuum and Power considerations

There are several considerations that must be made in designing a cavity for tests at high power (10s of kW). The cavity must be able to use a larger RF power source, instead of the small antennas used previously. The surfaces must be treated to avoid sparking. The cavity must also be able to withstand a good vacuum. The adhesive used to attach the dielectric to the copper tube should be replaced by a different method of attachment.

7.1.1 Ports

RF power is brought to the test hall through waveguides (described in Chapter 8). A coupler will need to be attached to the cavity in order to transition to a coaxial cable for delivering the RF to the cavity. The MTA has couplers used in other RF cavity tests, which will be reused for these tests. An example schematic can be seen in Figure 9-1, with a picture in Figure 7-2.

Because low power calibration tests must be performed on the cavity before the high power tests, additional RF ports will be required. These ports must not have sharp edges that would cause sparking.

The cavity must be treated before these tests. It will be cleaned and smoothed to

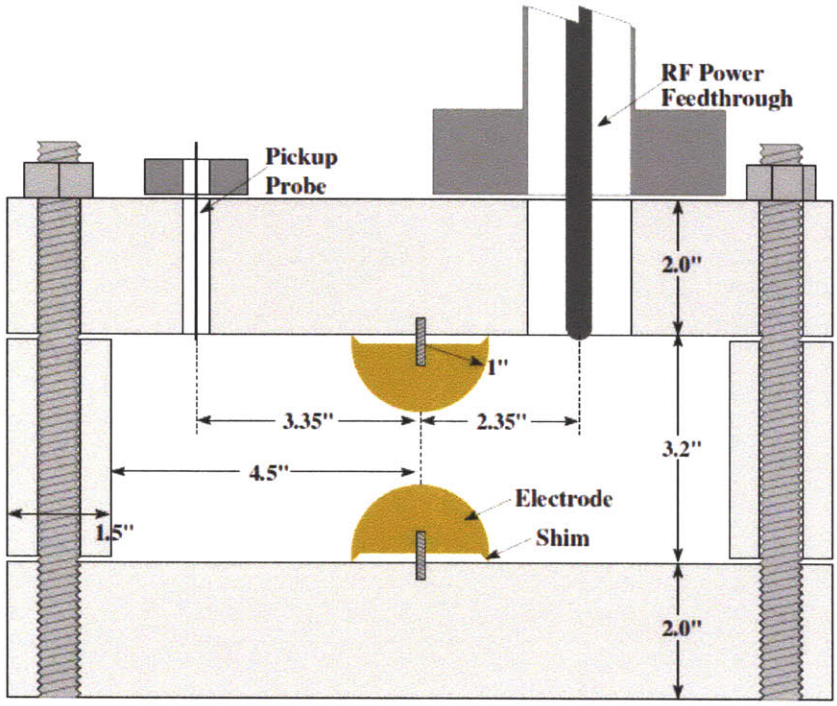

Figure 7-1: Example schematic of RF ports. The central knobs are for materials testing, and would not be included in this experiment. Image Source: Katsuya Yonehara.

remove any debris, imperfections, or grease from machining that could cause sparking in the tests. The ceramic must be separately cleaned using an ultrasonic cleaning method.

Vacuum ports will be required to pump the air out of the cavity for the tests. A vacuum of around 10^{-7} to 10^{-8} is desired.

An optical port is being considered, which would be used to observe any glow from the ceramic due to ionization.

Each of this ports will potentially shift the frequency and Q of the cavity, and must be carefully placed.

7.1.2 Construction

The ceramic will be held to the cavity by depositing a layer of copper on the edges, then welding this to the copper plates in the cavity. The adhesive used in the low power tests will be replaced in order to obtain a better vacuum. Outgassing from

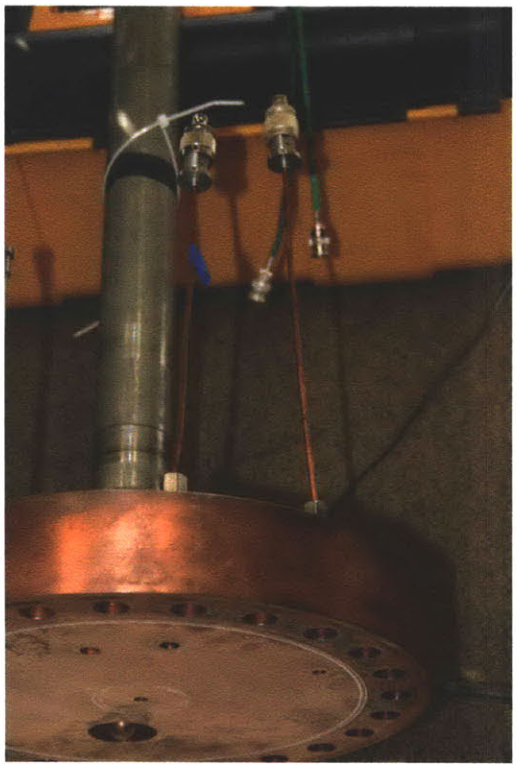

Figure 7-2: Photo of cavity described in Figure 9-1. Image Source: Katsuya Yonehara.

the adhesive could also contribute to sparking, especially since it is located in a high electric field region.

The initial tests of the cavity may show a need for redesign. The cavity shown in Figure 9-1 and 7-2 as shown is after many tests and revisions.

7.2 Importance of High Power Tests

In a muon collider, the cavity will need to operate with power on the order of 10s of kW. There are several types of behavior we expect to see in the high power tests that would not be observed in low power tests. The conductivity of the copper, the size of the cavity, and the dielectric constant of the ceramic will change with temperature. One difference between the high powered tests here and operation in a muon collider is the presence of cooling coils on the outside.

Many behaviors important to the operation of the cavity in a muon accelerator can only be observed accurately at high power, such as the breakdown point and the

Q, as well as the effects of heating in the ceramic.

7.3 Designs for Future Tests

There are several ideas for changes to this design, that would be worthwhile to test at a later date. One of these is filling the outer volume (separated from the beam by the ceramic) of the cavity with a dielectric liquid, such as oil. This would have similar benefits as the ceramic, in lowering the resonant frequency and preventing breakdown. Additionally, the oil could be circulated through the cavity to cool the ceramic.

More testing would be required to determine the operation of the cavity in cryogenic conditions. This would be required by the magnets in the final accelerator, and would also lower the resistance of the copper, leading to a higher Q. This cavity would not use oil, but instead a high pressure gas to remove the heat.

Further tests for the viability of this kind of cavity in a muon accelerator must include a test of whether or not a sustained gradient can be held in the presence of a magnetic field. The effects of beam loading must also be determined [7]. This is a multi-year project, but will be critical to the operation of a muon accelerator if the cavity is able to solve the problem of suppressed gradients in a magnetic field.

Chapter 8

Muon Test Area

The Muon Test Area (MTA) [15] [17] is a facility at Fermilab designed to test various technologies for developing a muon collider. It is located next to the Linac, the first step of particle acceleration at Fermilab. The MTA makes use of a 400 MeV proton beam from the Linac. The facility is underground, and the ground level can be seen in Figure 8-2, with Wilson Hall in the background. The beamline is shaped by several magnets, as seen in Figure 8-3. The proton beam will not be used for this stage of the experiment. However, the solenoid and RF power will be used. Seen as viewed along the beamline, the solenoid and RF power feed can be seen in Figure 8-4. The facility has the capability of using both 201 and 805 MHz RF power. 805 MHz power will be used in this experiment.

RF power to the facility is produced by klystrons along the Fermilab Linac. It is fed into the hall with waveguides, seen in the schematic in Figure 8-1. The 201 MHz RF is at 4.5 MW, and the 805 MHz RF is at 12 MW.

The facility has several detectors available for use. There are ionization counters, plastic scintillation counters, and a crystal scintillation counter. There are also vacuum instrumentation and optical fiber probes. The use of these detectors for this experiment will be described further in Chapter 9.

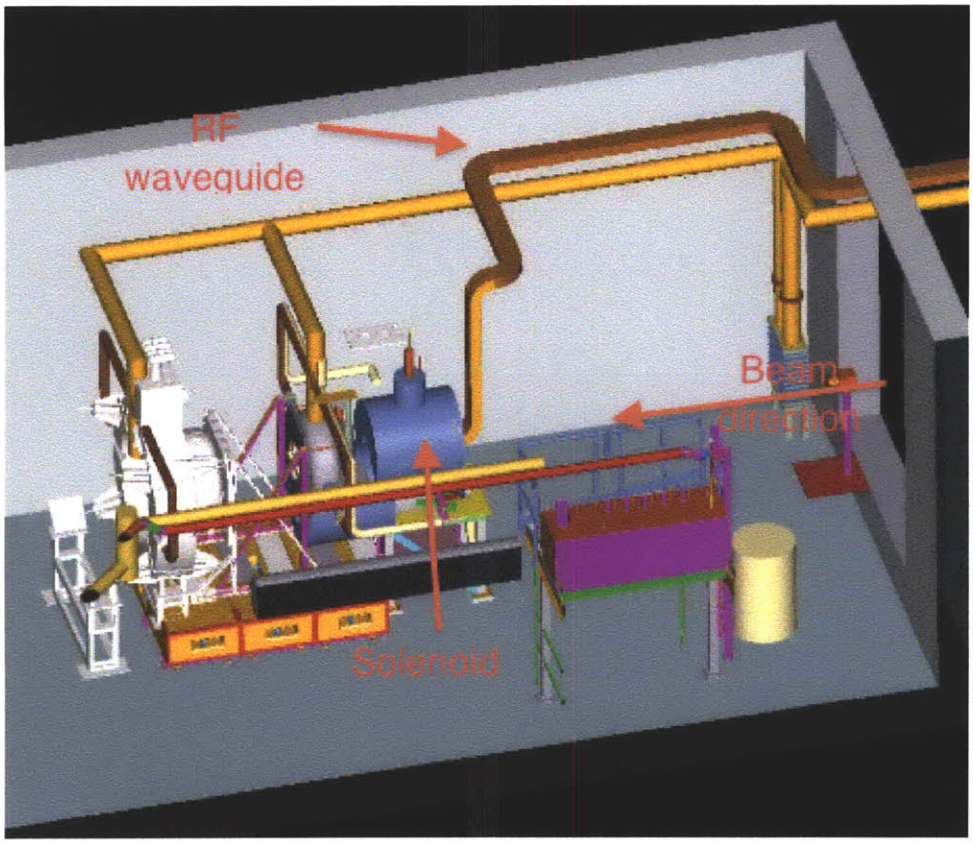

Figure 8-1: Schematic of MTA Experimental Hall (Image source: [17])

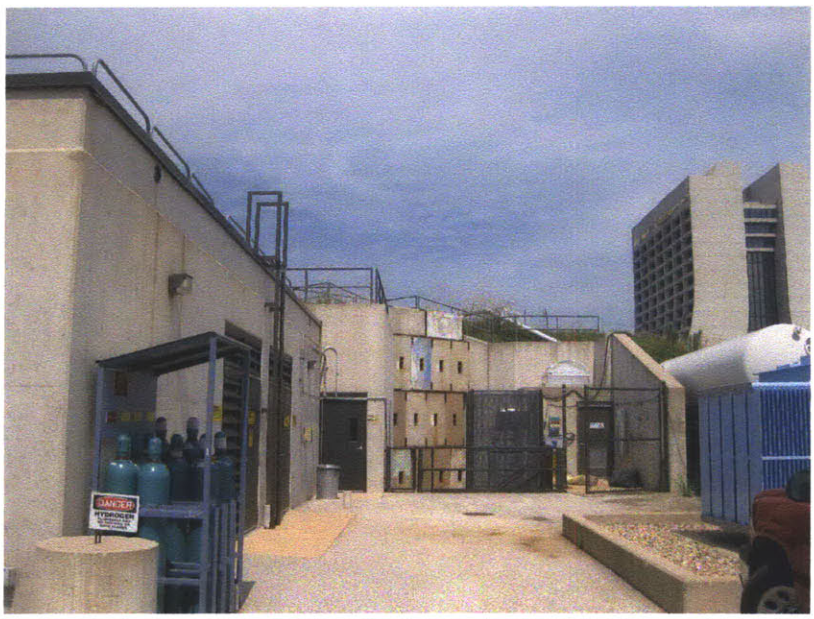

Figure 8-2: Ground level view of MTA.

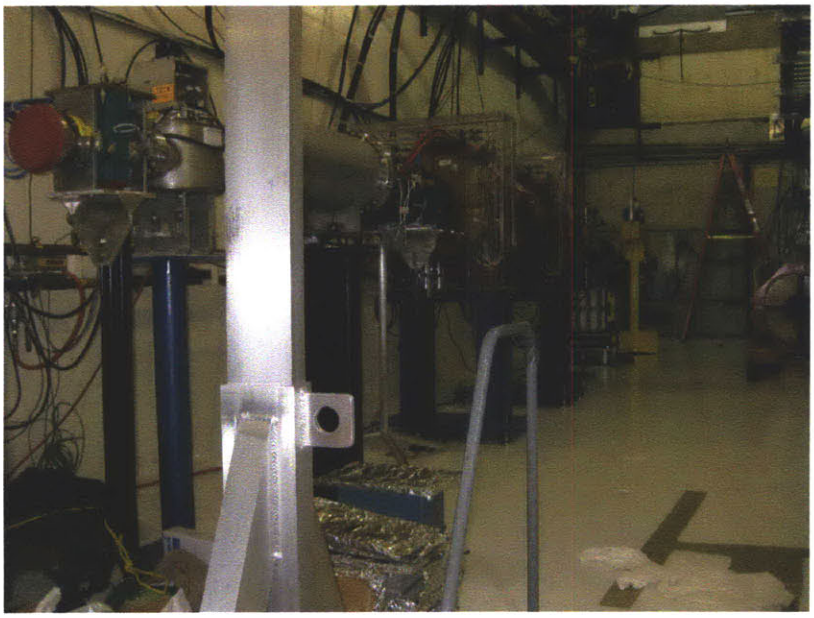

Figure 8-3: MTA beamline

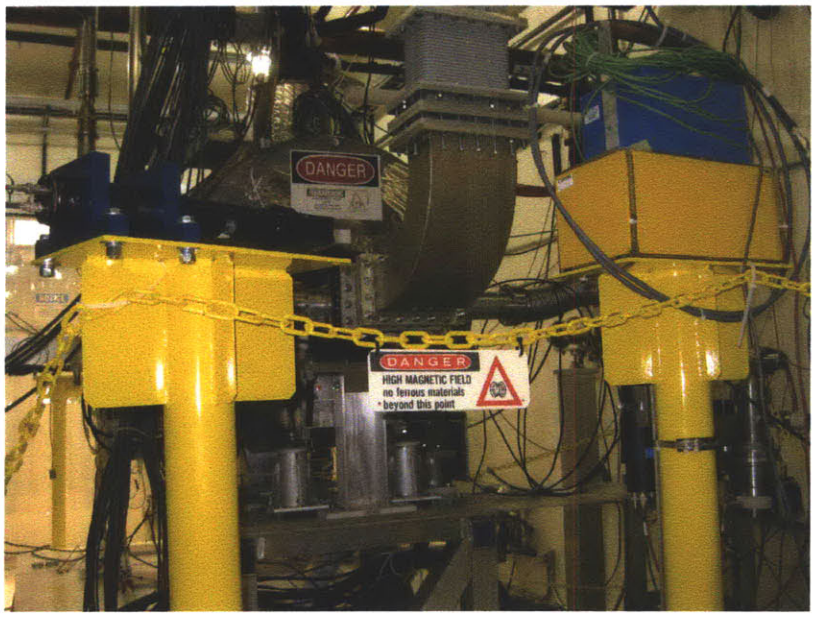

Figure 8-4: Front view of solenoid and RF power feed in MTA. For orientation, the beamline comes from the back right in this picture.

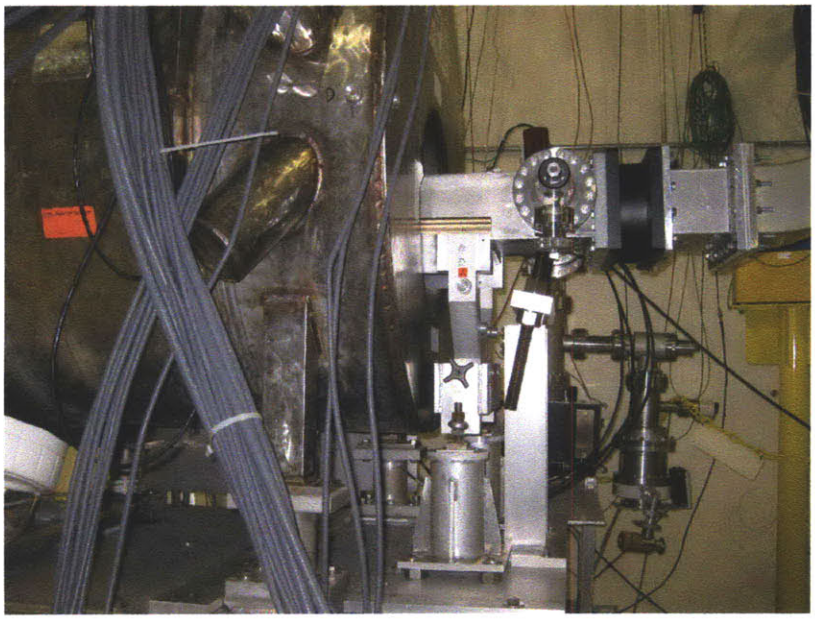

Figure 8-5: Closer view of solenoid, from the side.

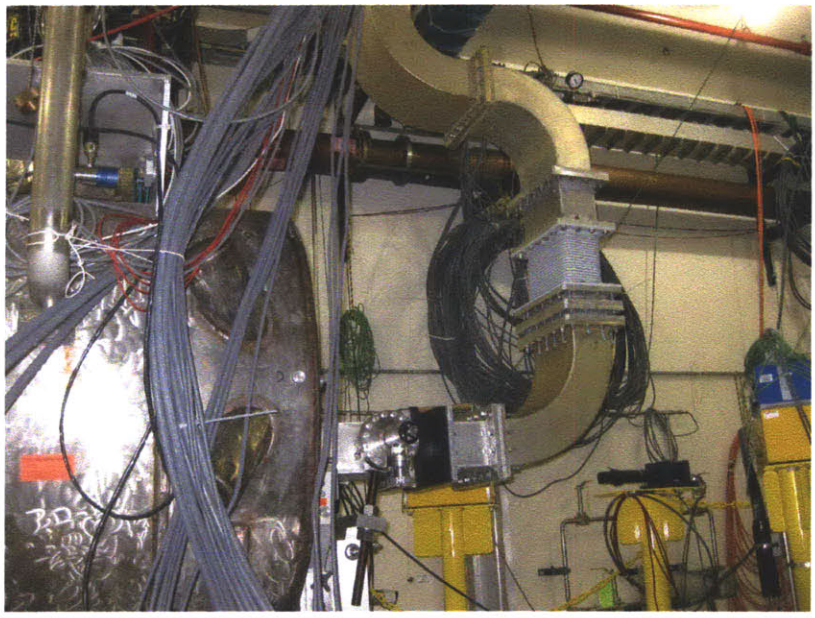

Figure 8-6: Closer view of solenoid and RF feed, again from the side.

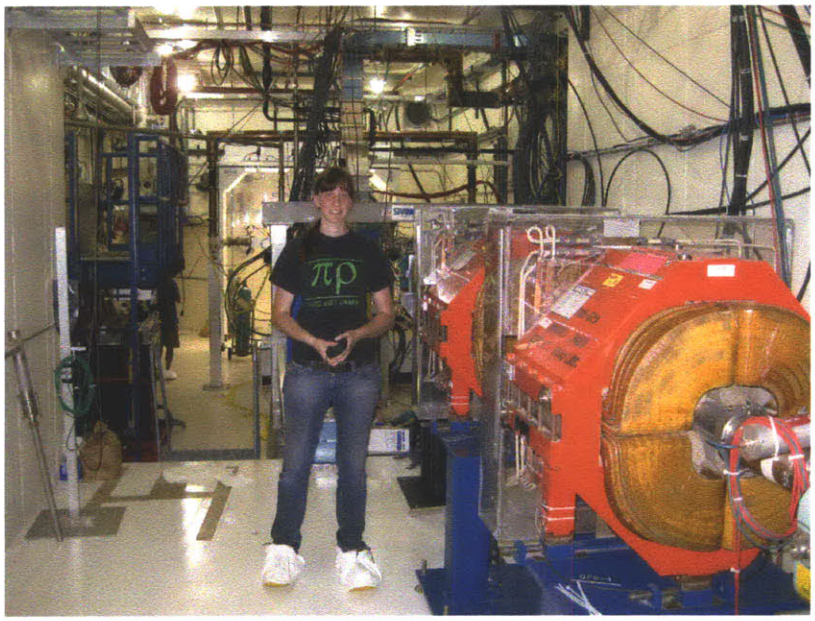

Figure 8-7: Thesis author, in the MTA Experimental Hall.

Chapter 9

High Power Tests of Cavity

High power tests of the cavity are planned for the MTA, described in the previous section. Due to the time constraints of this work and of the facility's schedule, these tests have not been carried out. In this section, the planned tests are described for the benefit of those who would like to further this project.

Similar tests of RF cavities at the MTA are described in [20] and [16]. An example schematic of one such test is shown in Figure 9-1. The test described in [20] is for a pressurized cavity, and the procedure for this cavity would need to be modified to vacuum seal the cavity. However, the important features of the schematic relevant to these tests are the RF power input from the Klystrons, the PMT to detect breakdown, the probe to observe the fields inside the cavity, and the computer control system.

9.1 Conditioning

While the cavity will be cleaned prior to the tests, it must be conditioned to remove the rest of the debris, grease, and imperfections on the interior surfaces. The power level must be increased slowly, so that these imperfections are cleared with low power sparks. This is standard procedure for RF cavities prior to operation at some higher power level.

We will start by applying RF power to the cavity in short bursts. The length of these bursts is determined by the fillup time of the cavity, which is proportional to

the Q. If the Q is 10,000, the burst lengths will be less than 5 μs. The muon beam eventually used will only be a few nanoseconds long, so a long sustained RF is not required. Because the cavity will not yet have any cooling mechanism at this testing stage, the bursts must be infrequent as to not overheat the ceramic. We will start with a burst frequency of around 1 Hz. Over the course of 1-2 weeks, the amplitude and duration of the bursts will be slowly increased to full power.

9.2 Quantities Monitored During Tests

One important diagnostic during the test is the directional coupler inside the waveguide (not shown in Figure 9-1). This provides signal for the forward and reflected power, which will indicated how much power is sent to the cavity, and how much goes in.

The vacuum will be monitored, and will indicate any sparking. Large changes will indicate breakdown, and a slow degradation of the vacuum will indicate that the power is too high for the conditioning of the cavity. The slow degradation is due to sparking, as well as dark current.

If an optical port is installed, that will be monitored as well. The signal for a sample breakdown event can be seen in Figure 9-2.

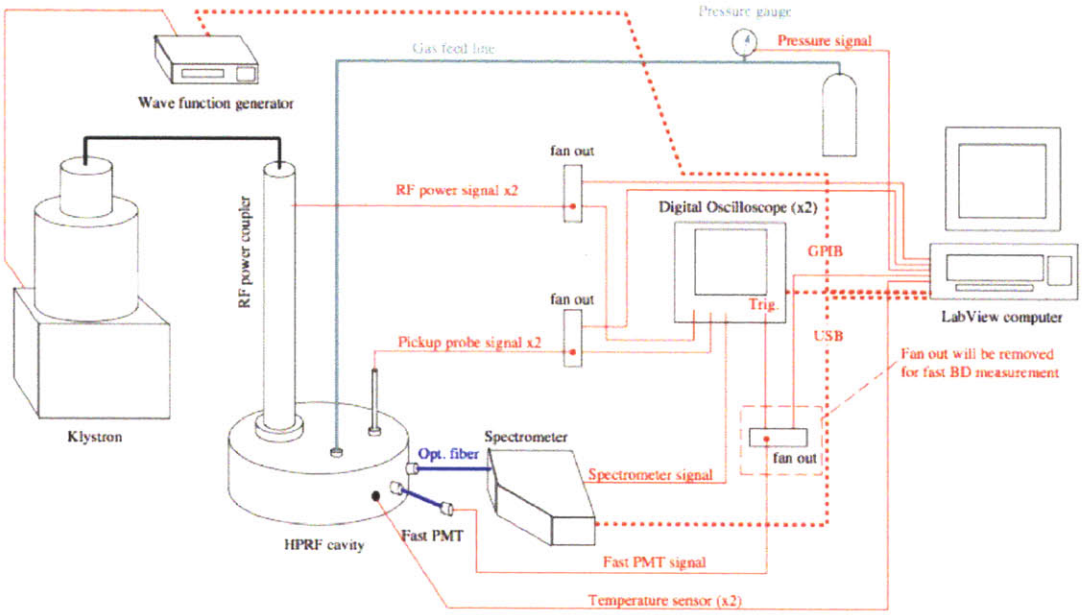

Figure 9-1: Example Schematic of High Powered Tests at the MTA(Source: [20])

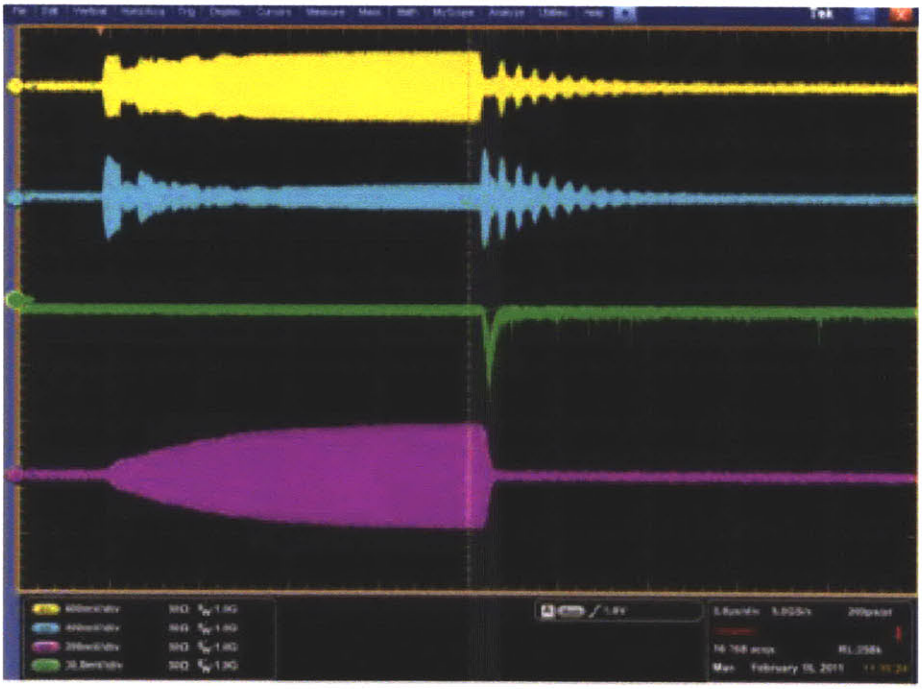

Figure 9-2: Sample observation of a breakdown event. From top to bottom, the signals are: forward RF power, reflected RF power, PMT signal, and electric pickup (Source: [7]).

Chapter 10

Conclusions

A dielectric-loaded RF cavity was designed and tested at low power, and high power tests were planned. The goal of the dielectric cavity is to reduce the breakdown in the cavity when operated inside of a magnetic field, as well as to allow for a smaller cavity for a given RF frequency. Several prototype cavities were designed in Microwave Studio, built, and tested using a network analyzer to measure their lowest mode frequency and Q value. An offset from the frequency predicted by the Microwave Studio simulations was observed, and is discussed in Chapter 6. The measured Q values were limited by the construction of the cavity. The next stage in testing procedures is to make similar tests at high power. The design considerations for the high power tests include adapting the cavity for a larger RF port, a vacuum, and using a new method to attach the dielectric. In order to eventually prepare a dielectric cavity for consideration in a muon accelerator, high power tests in a high magnetic field will be necessary. Many possible alterations in the design could possibly make the cavity even less likely to experience breakdown at a low electric field than the pillbox-shaped cavity studied in this thesis.

Bibliography

[1] Ad-995 alumina material properties. http://www.coorstek.com/materials/ceramics/alumina/ad995.asp, 2010.

[2] V. Barger, M. S. Berger, K. Fujii, J. F. Gunion, T. Han, C. Heusch, W. Hong, S. K. Oh, Z. Parsa, and S. Rajpoot. Physics goals of a mu(+) mu(-) collider. In *Presented at the 2nd Workshop on Physics Potential and Development of Mu(+) Mu(-) Colliders, Sausalito, CA, 17-19 Nov. 1994*, pages 17–19, March 1995.

[3] W. Barletta. US Particle Accelerator School Notes, 2010.

[4] J. D. Cockcroft and E. T. S. Walton. Experiments with high velocity positive ions. (i) further developments in the method of obtaining high velocity positive ions. *Proceedings of the Royal Society of London. Series A, Containing Papers of a Mathematical and Physical Character*, 136(830):pp. 619–630, 1932.

[5] CST Microwave Studio Manual. Accessed: July, 2010.

[6] Yaroslav Derbenev and Rolland P. Johnson. Six-dimensional muon beam cooling using a homogeneous absorber: Concepts, beam dynamics, cooling decrements, and equilibrium emittances in a helical dipole channel. *Phys. Rev. ST Accel. Beams*, 8(4):041002, Apr 2005.

[7] B. Freemire, P. M. Hanlet, D. Kaplan, Y. Torun, M. R. Jana, A. Moretti, M. Popovic, A. V. Tollestrup, K. Yonehara, G. Flanagan, R. P. Johnson, and M. Notani. High pressure rf cavity test at fermilab. *Proceedings of PAC11*, 2011.

[8] J. Gallardo, R. Palmer, A. Tollestrup, A. Sessler, and A. Skrinsky et al. Mu+ - Mu- Collider: A Feasibility Study. In *Proceedings of the 1996 DPF/DPB Summer Study on New Directions in High-energy Physics*, 1996.

[9] D. Neuffer. Principles and applications of muon cooling. In *American Institute of Physics Conference Series*, volume 352 of *American Institute of Physics Conference Series*, pages 12–15, January 1996.

[10] V. V. Parkhomchuk and A. N. Skrinsky. Ionization cooling: Physics and applications. In *American Institute of Physics Conference Series*, volume 352 of *American Institute of Physics Conference Series*, pages 7–9, January 1996.

[11] M. Popovic. Personal communication, 2010.

[12] M. Popovic, A. Moretti, C. Ankenbrandt, M. Cummings, R. Johnson, and M. Neubauer. Dielectric loaded rf cavities for muon facilities. *Proceedings of IPAC10, Kyoto, Japan*, 2010.

[13] D. Pozar. *Microwave Engineering.* Wiley, third edition, 2005.

[14] A. N. Skrinsky and V. V. Parkhomchuk. Cooling methods for beams of charged particles. *Sov. J. Part. Nucl.*, 12:223, 1981.

[15] Y. Torun. Mucool test area, http://mice.iit.edu/mta/, January 2011.

[16] Y. Torun, D. Huang, J. Norem, A. Bross, M. Chung., A. Jansson, A. Kurup, J. Misek, and A. Moretti. Rectangular box cavity tests in magnetic field for muon cooling. *Proceedings of IPAC10, Kyoto, Japan*, 2010.

[17] Y. Torun, D. Huang, J. Norem, R. Palmer, D. Stratakis, A. Bross, M. Chung, A. Jansson, A. Moretti, K. Yonehara, D. Li, and R. Rimmer. The mucool test area and rf program. *Proceedings of IPAC10, Kyoto, Japan*, 2010.

[18] D. Valuch. Radio frequency systems of the cern synchrotron accelerators. In *Radioelektronika, 2009. RADIOELEKTRONIKA '09. 19th International Conference*, pages 17 –24, 2009.

[19] R. Vila, M Gonzlez, J. Moll, and A. Ibarra. Dielectric spectroscopy of alumina ceramics over a wide frequency range. *Journal of Nuclear Materials*, 253(1-3):141 – 148, 1998.

[20] K. Yonehara. High Pressurizing Hydrogen Gas Filled RF Cavity test, September 09 run. *Muons, Inc*, 2009.

[21] K. Yonehara, R. P. Johnson, M. Neubauer, and Y. S. Derbenev. A helical cooling channel system for muon colliders. *Proceedings of IPAC10, Kyoto, Japan*, 2010.